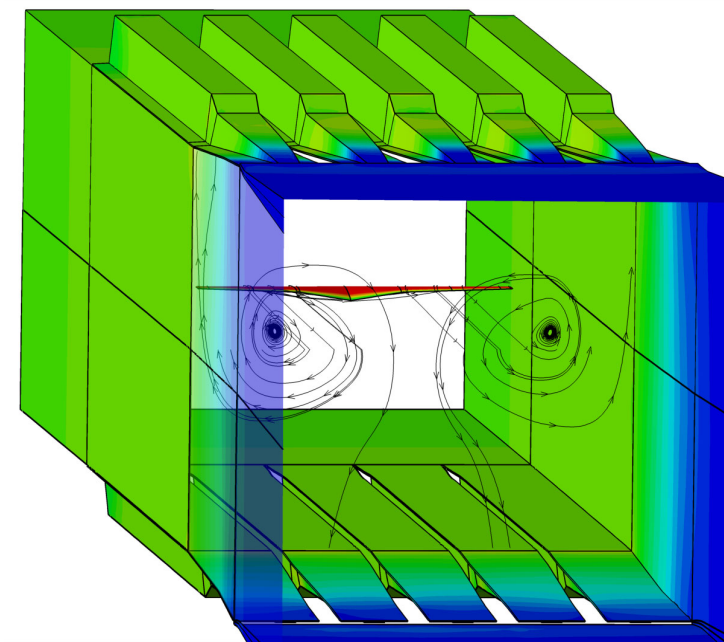## Executive summary

Development of CFD-based interference models for the DNW-HST transonic wind tunnel

Problem area
Advances in CFD technology have enabled the simulation of the complex internal flow field of a transonic wind tunnel. Wall and model support interference models for low speed wind tunnels featuring test sections with solid walls are relatively well developed. However, the geometrical complexity of slotted walls and the associated flow features complicates the development of interference models for transonic wind tunnels. A phased approach has therefore been adopted for the development of wall and sting

interference models for the DNW-HST transonic wind tunnel.

Description of work
The present work constitutes the first development phase and provides a CFD model of a wind tunnel that consists of a test section with longitudinally slots, a plenum chamber and a section of the downstream diffuser. The objective is to understand the tunnel flow characteristics and to verify the computed slotted wall interference effects in a systematic study by considering an isolated wing at different model sizes.

This report is based on a presentation held at the 25th AIAA Aerodynamic Measurement Technology and Ground Testing Conference, San Francisco (U.S.A.), June, 2006.

Results and conclusions

Multi-block structured grid technology is applied to construct a numerical model of the wind tunnel. Turbulent flow simulations are performed to calculate the transonic flow in the test section, subjected to interactions with the stagnant air in the surrounding plenum chamber. The predicted empty test section flow characteristics show good agreement with proprietary tunnel calibration data, in terms of horizontal buoyancy. Consistent wall interference effects are found in a comparison of the aerodynamic characteristics of the test article in the tunnel environment and in free air. The drag increment due to wall interference associated with increasing model scale is assessed for test articles sizes beyond commonly accepted values.

Applicability

The purpose of the present effort is to support wind tunnel testing activities. The numerical model of the wind tunnel can support investigations to improve the accuracy of measurements or in decision making with respect to the industrial pull to test at the largest possible model size. The present results encourage the inclusion of the model support system in the established CFD representation of the wind tunnel in the next development phase in order to account for sting interference effects.

Nationaal Lucht- en Ruimtevaartlaboratorium
National Aerospace Laboratory NLR

NLR-TP-2006-504

Development of CFD-based interference models for the DNW-HST transonic wind tunnel

J.E.J. Maseland, M. Laban, H. van der Ven and J.W. Kooi

Customer	DNW
Contract number	DNW Purchase Order 15.0006
Owner	NLR
Division	Aerospace Vehicles
Distribution	Unlimited
Classification of title	Unclassified
	January 2007

Approved by:

Author	Reviewer	Managing department
20/2/08	ML 20/2/2008	22/2/2008

Contents

Development of CFD-based interference models for the DNW-HST transonic wind-tunnel

J.E.J Maseland, M. Laban , H. van der Ven

National Aerospace Laboratory NLR, Amsterdam, The Netherlands

J.W. Kooi

German-Dutch Wind Tunnels DNW, Emmeloord, The Netherlands

Advances in CFD technology have enabled the simulation of the complex internal flow field of a transonic wind-tunnel. The ENFLOW CFD system of NLR has been applied to calculate the flow about models of various size placed in the DNW-HST transonic wind-tunnel.

The primary objective of the present work is to provide a CFD model of a tunnel representation that consists of the slotted test section, plenum chamber and diffuser. The aim is to understand the tunnel flow characteristics and to determine the slotted wall interference effects with increasing test article size, up to values beyond commonly accepted limitations. The modelling activities for turbulent flow simulations based on multi-block structured grid technology include exploratory empty tunnel flow calculations for a Mach number $M_\infty=$ 0.80 and a unit Reynolds number $Re_\infty=$ 20 million. The predicted horizontal buoyancy characteristics are compared to measured characteristics in available test section calibration data. The lessons learned for flow modelling are then applied to simulate the tunnel flow about an isolated DLR-F4 wing featuring a wing span of 70%, 80% and 85% of the wind-tunnel width. The wind-tunnel wall interference is assessed in a comparison with free air simulations of the test article.

It is concluded that the developed numerical model predicts consistent wall interference effects for a slotted tunnel and that the present results encourage the inclusion of the model support system in the CFD model to account for sting interference effects in the next development phase.

List of symbols

B	wind-tunnel test section width	[m]
b	wing span	[m]
C_D	drag coefficient	[-]
C_L	lift coefficient	[-]
C_p	pressure coefficient	[-]
H	wind-tunnel test section height	[m]
M	Mach number	[-]
Re	Reynolds number	[-]
S	reference wing area	$[m^2]$
α	angle of incidence	[degrees]
η	normalised span-wise coordinate; $y/(b/2)$	[-]

subscripts
∞	free stream value	

Abbreviations
CFD	Computational Fluid Dynamics
DNW	German-Dutch Wind Tunnels
HST	High-Speed Wind-Tunnel

I.   Introduction

Ventilated wall wind-tunnels are in use for over decades and have proven to be effective in reducing wall interference effects at low and transonic speeds. The sign reversal of wall corrections for open and closed test sections enables a carefully designed ventilated test section to reduce both magnitude and inhomogeneity of wall corrections for large models and high lift coefficients. The High Speed Tunnel (HST) in Amsterdam, The Netherlands, operated by the German-Dutch Wind Tunnels (DNW) is an example of a wind-tunnel with ventilated walls. The DNW-HST is a variable-density closed-circuit continuous wind-tunnel with streamwise slotted ceiling and floor test section walls (12% open ratio per wall). The test section has a rectangular cross section 2.0 (m) wide by 1.6 (m) or 1.8 (m) high. The larger height is used mainly for high incidence and supersonic testing. The slots allow for streamline divergence into a large plenum chamber that surrounds the test section (see figure 1). The plenum air is passively vented into the downstream part of the test section. High Reynolds number testing is enabled by pressurisation of the tunnel up to values of 390 kPa.

State-of-the-art CFD methods are capable to model the flow field about test articles placed in a wind-tunnel. The advantage of such CFD calculations is the possibility to compare the numerical results for the wind-tunnel environment to results of free air simulations in order to estimate wind-tunnel interference effects. The simulation of the internal flow in non-ventilated test sections is well defined as the solid walls have a zero normal flow at the wall. The wall and sting interference models for closed test sections are therefore well-developed and validated. For ventilated test sections with partly solid and open walls, the geometrical complexity of the wind-tunnel wall and associated flow features complicate the development of interference models. The effect of the wall openness may either be modelled using porous boundary conditions or by modelling the viscous flow through the slots based on physical boundary conditions. In the latter case, the actual slot geometry is part of the computational domain. Nevertheless, the accurate modelling of the flow with a large disparity in scales related to speed and total pressure, free shear layer flow and partly separated flow areas remains a challenging task.

The industrial pull to improve the accuracy of force measurements, the surface representation of models and the viscous effects characterised by high Reynolds numbers leads to largest possible test articles. Wall interference can become a limiting factor on the size of the models. The objective of the present work is develop CFD based interference models for the DNW-HST tunnel and assess the predictive capability for wall interference associated with increasing model size. For this purpose, a computational model of the DNW-HST tunnel representation is developed covering the test section, surrounding plenum chamber and diffuser. The computed empty tunnel flow is analysed and compared to available tunnel calibration data. Subsequently, the transonic flow in the DNW-HST tunnel is modelled including an isolated test article (DLR-F4 wing) featuring a wing span of 70%, 80% and 85% of the tunnel width. The wind-tunnel wall interference with increasing model size is assessed in a comparison with free air simulations for the test article.
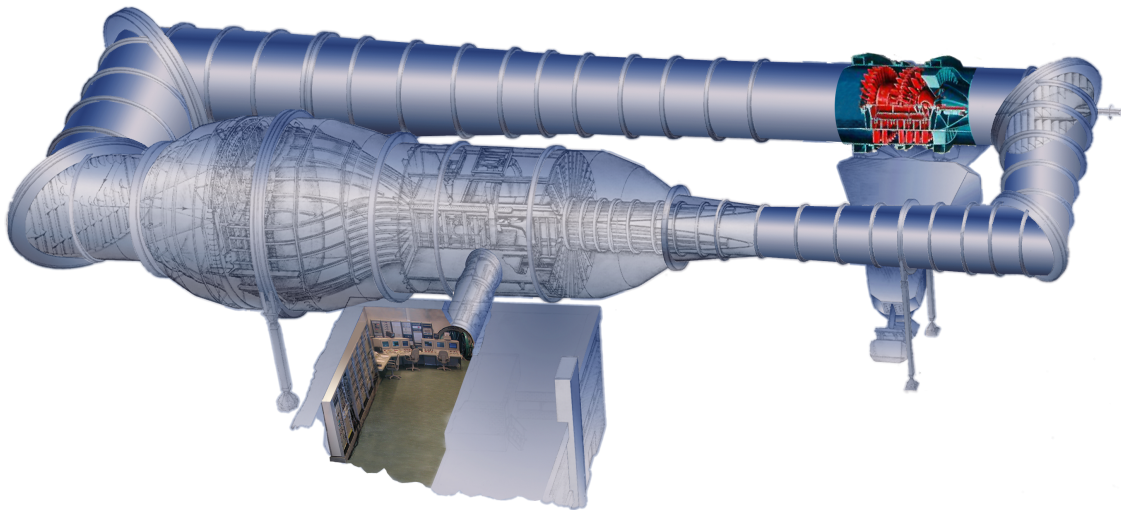

Figure 1. High Speed Tunnel (HST) at DNW-Amsterdam site

II.   Numerical approach

The result of numerical simulations have been obtained by using NLR's ENFLOW system [Boerstoel[1]]. The ENFLOW system is the in-house developed multi-purpose CFD-system suitable for solving either the Euler or Navier-Stokes flow equations on multi-block structured meshes from incompressible flow to supersonic flow. State-of-the-art two-equation turbulence models are available for efficient and accurate representation of turbulence in a Reynolds-averaged fashion. The ENFLOW system has been extensively employed for a wide range of applications ranging from internal cabin flow analyses up to aero-elastic studies for very large transport aircraft at transonic speeds.

The computational meshes for the tunnel flow analyses are created by applying boundary-layer blocks on each solid wall component of the solid and slotted tunnel walls, the plenum chamber, the diffuser and the test article. The tunnel geometry definitions for the contraction cone and the settling chamber are not used in the CFD model. These relatively complex geometrical parts are replaced by an upstream extension of the square test section geometry.
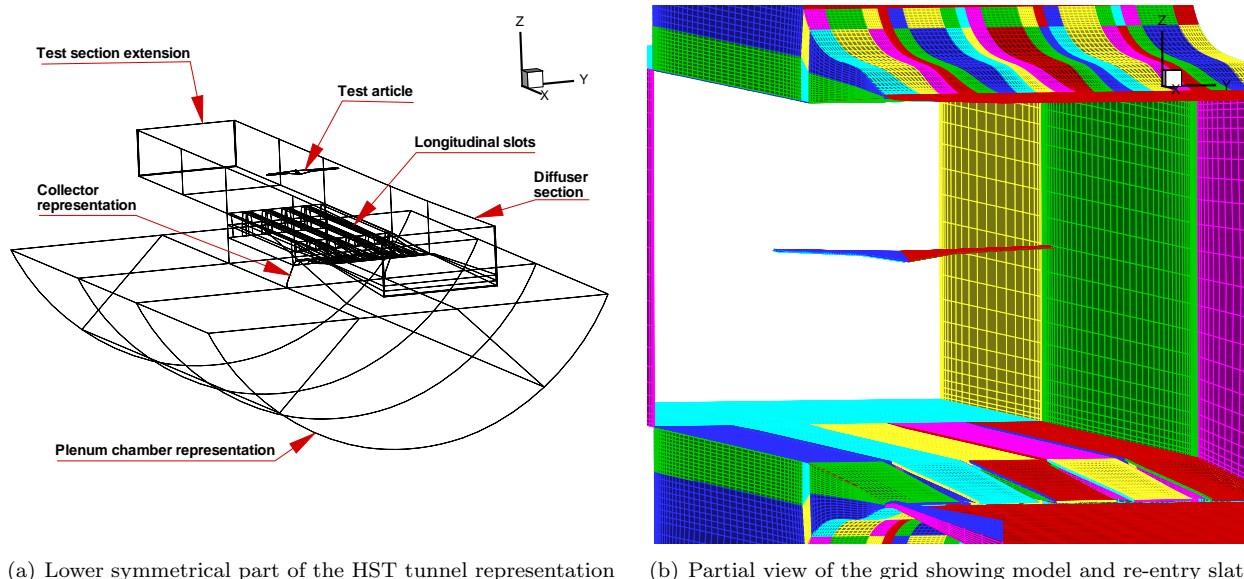

(a) Lower symmetrical part of the HST tunnel representation   (b) Partial view of the grid showing model and re-entry slats

Figure 2. CFD representation of the HST Wind Tunnel including the test section, plenum chamber and diffuser section

The surface geometry is subdivided into a set of faces according to a selected topological decomposition of the flow domain. Views of the resulting surface decomposition for the entire tunnel and test section are presented in figure 2 Blocks are generated in the flow domain using the domain decomposer ENDOMO. Grid control parameters are set using the interactive grid generator ENGRID [Spekreijse[2]]. The resulting computational domain consists of 712 blocks containing 5.2 million grid points.

The flow analysis is fully viscous and the selected flow model is based on the full Reynolds-Averaged Navier-Stokes equations. Turbulence is taken into account by employing a two-equation $k - \omega$ turbulence model with enhancements for flows with separated regions [Kok[3]].

III.   Simulation of empty test-section flow

Exploratory calculations are carried out to characterise the wind-tunnel flow for an empty test section at a Mach number $M_\infty = 0.80$ and a Reynolds number $Re_\infty = 20$ million per meter. The virtual origin of the turbulent boundary layer on the solid walls of the square test section extension is located at 2.5 meters upstream of the slots. The flow in the test section is analysed by extracting the pressure coefficient and Mach number distribution at the tunnel centre-line and at a vertical trace passing through the model centre. (see figure 3). The Mach number distribution at the vertical trace shows a constant value at the core of the test section with a local maximum near the walls. The pressure coefficient distribution along the tunnel centre-line in figure 3b illustrates the elevated pressure level on the upstream wall extensions due to the

displacement effect of the boundary layer on the solid walls. This level is gradually reduced by the presence of the slots (x≥-1200) to values with very small deviations from the plenum pressure. Above the re-entry slats (x≥ 2200), the effect of the diffuser section is recognised by the sudden increase in values of the pressure coefficient. The distribution of the pressure coefficient in the test section is very similar to empty tunnel calibration measurements [Wubben[4]] in terms of the absolute level and the pressure gradients.

(a) Tunnel centre-line trace

(b) Tunnel centre-line trace
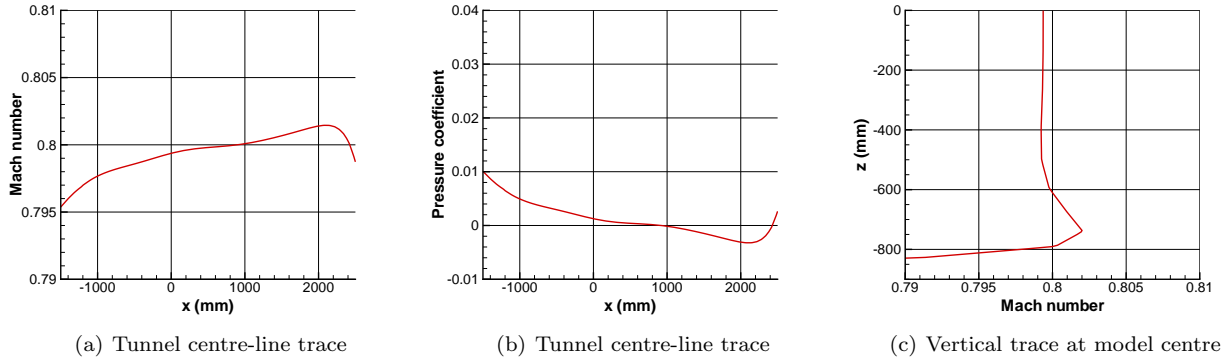
(c) Vertical trace at model centre

Figure 3. Pressure coefficient and Mach number distribution in the empty tunnel at Mach= 0.80

The flow in the test section and part of the plenum chamber is presented in a plane perpendicular to the tunnel axis which is located at the model position, i.e. x=0. Figure 4 shows the distribution of the the non-dimensional vertical velocity component (normalised by U_∞) and the pressure coefficient. The tunnel flow enters the plenum chamber as a free jet [Bernt,[5] Everhart[6]]. The flow through the slots sets-up a secondary flow in the plenum chamber. The variation in transverse flow through the individual slots introduces a swirling flow structure in the plenum chamber. The corresponding pressure coefficient distribution depicts the pressure drop in the slots.
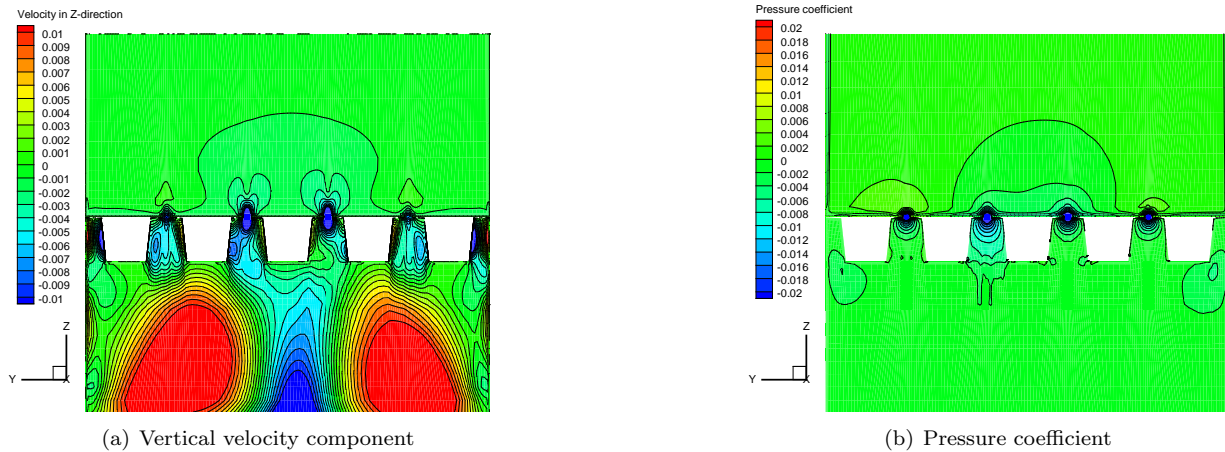

(a) Vertical velocity component

(b) Pressure coefficient

Figure 4. Empty tunnel flow field at model position for Mach= 0.80

IV. Simulation of wind tunnel flow about wing models of various size

The flow in the tunnel is subsequently simulated for an isolated test article at different model scales. The test article is the DLR-F4 wing configuration featuring a full-span of 70%, 80% and 85% of the wind-tunnel width. Characteristics of the tunnel flow in stream-wise direction are discussed by considering the longitudinal and transversal velocity component distributions for a section located at y=-200 (mm) from the tunnel centre-line in figure 5. For this particular choice, the flow in the vertical symmetry plane of a slot is part of the investigation. The empty tunnel distribution is included in the figure as a non-lifting reference

solution to facilitate the identification of lift effects.

The longitudinal velocity distributions show the large variation of air speed ranging from incompressible flow in the plenum and compressible transonic flow in the test section. Large gradients are observed at the location of the slots where the test section flow interacts with the plenum air. Comparison of the individual longitudinal velocity distributions shows the increase of the footprint of the deflected wake near the tunnel centre-line with the increase in lift force related to the enlarged test article size. The curvature of the tunnel flow can be deduced from the gradients in the longitudinal velocity plots and suggests that the tunnel flow is deflected by the lifting test article. The grid-lines of the domain decomposition depict the slot depth and the height of the wall beams. Observe that the vertical extent of the interaction region of tunnel flow and plenum air is confined by the slots and the beams.
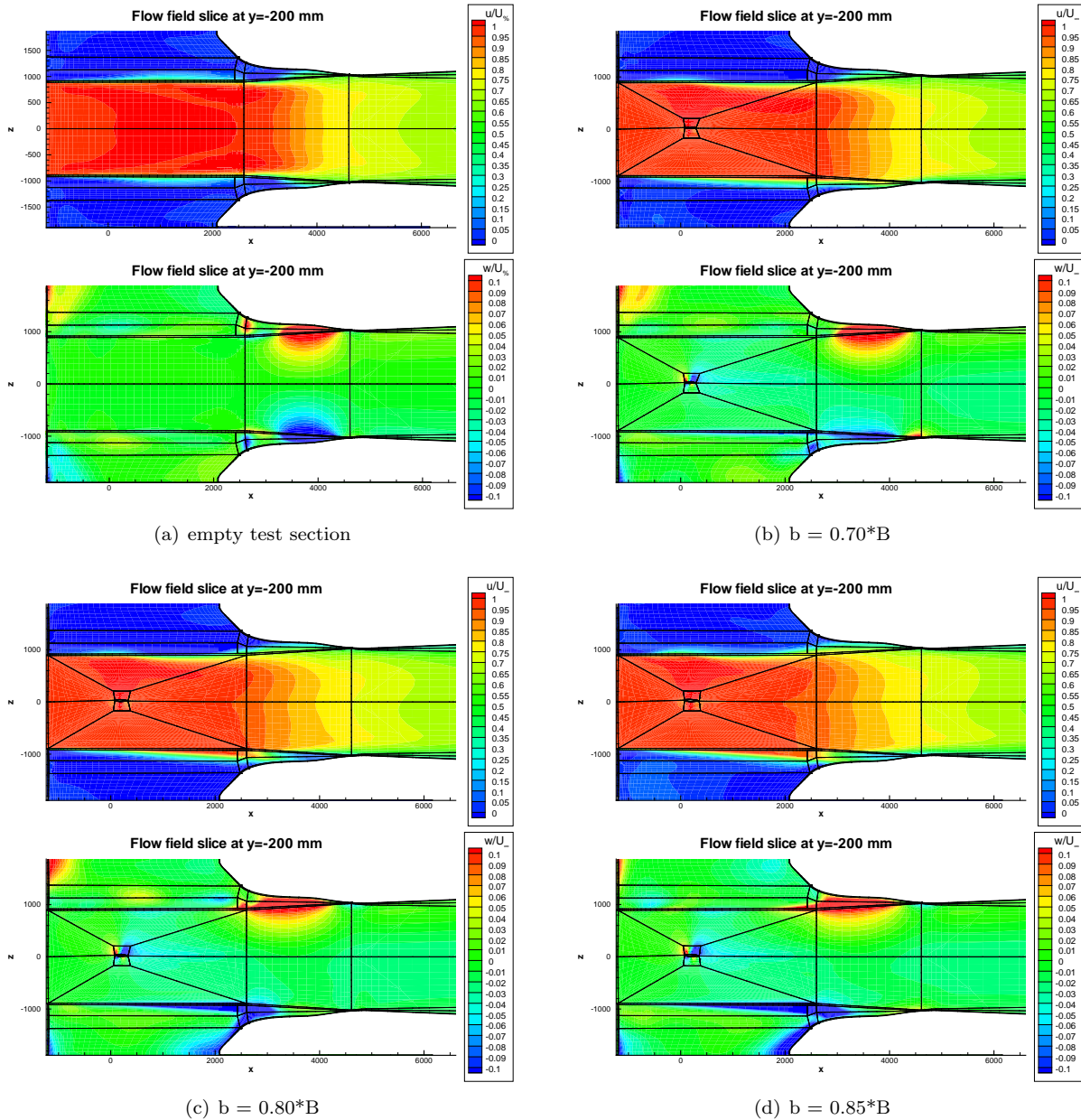

(a) empty test section

(b) b = 0.70*B

(c) b = 0.80*B

(d) b = 0.85*B

Figure 5. Tunnel flow curvature and normal flow through the slots for various model size

The actual flow into and out of the plenum through the longitudinally slots is indicated by the sign of the transversal component of the velocity. The inflow and outflow pattern for the slot in the upper test section wall corresponds to a streamline curvature of the tunnel flow. The slot in the lower test section wall shows a

9

predominant inflow pattern to the plenum implying a superposition of streamline curvature and downward deflection of the tunnel flow.

The distribution of the pressure coefficient on the tunnel walls is presented in figure 6. In general, the pressure coefficient distributions on the slotted ceiling and floor walls as well as the side-walls show a lift interference pattern. The slotted ceiling wall of the tunnel shows an increase in velocity due to the positive longitudinal perturbation velocities associated with the lift on the test article. On the lower slotted tunnel wall, these perturbation velocities change sign and result in an decrease of the tunnel velocity represented by small positive values for the pressure coefficient. The distributions on the side walls give an impression of the pressure coefficient gradients in the vertical direction. The lift interference effect results in an increase above the model and an decrease in velocity below the model. The small irregularities near the cusped slot entrance relate to an unsteady centrifugal force associated with the local streamline curvature.
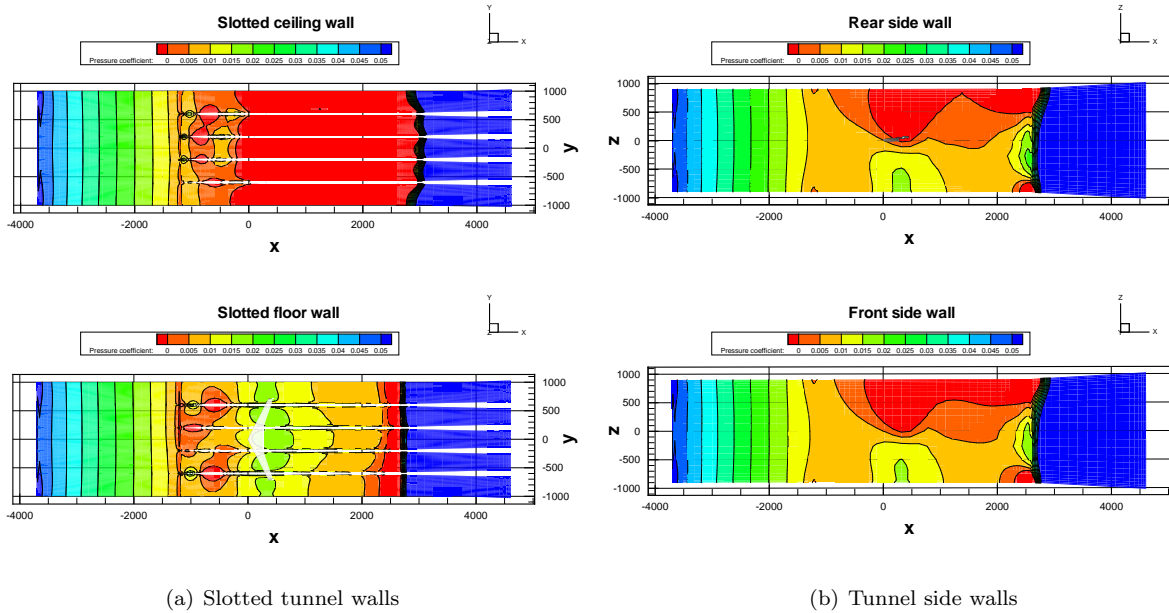

(a) Slotted tunnel walls

(b) Tunnel side walls

Figure 6. Pressure coefficient distribution on the tunnel walls for the 0.70*B span wing model

The wall signature in terms of the extracted pressure coefficient at the centre-line of the individual walls is presented in figure 7. The lift interference effect is again apparent in the curves for the ceiling and floor tunnel walls. Moreover, the wake blockage can be identified by the lack of pressure recovery and the resulting pressure coefficient difference between the mentioned curves.
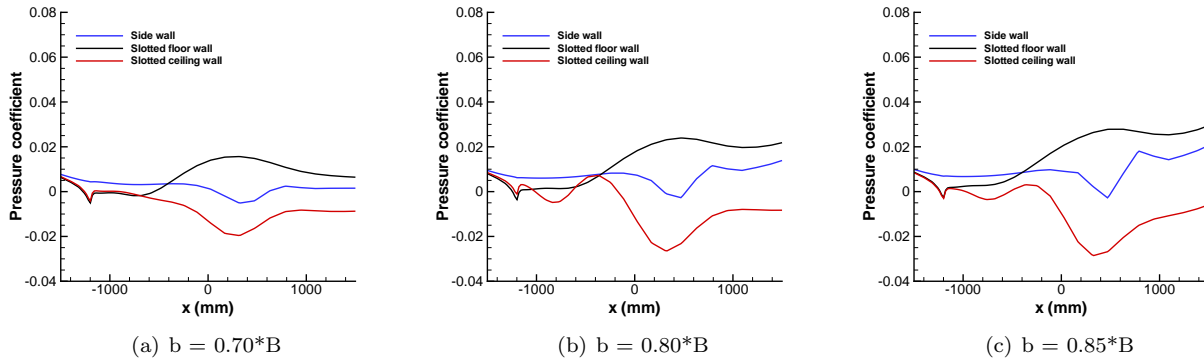

(a) b = 0.70*B

(b) b = 0.80*B

(c) b = 0.85*B

Figure 7. Pressure coefficient distribution on the tunnel wall centre-line for wing models of various size

V. Wall interference assessment in comparison to free air simulations

The wall interference is assessed by comparing results of free air simulations and flow calculations of the same wing in the tunnel. The computational grids for the free air simulations include the grids of the tunnel test section in order to ensure that the grid characteristics are identical for the spatial domain that covers the wind tunnel test section. The artificial far field boundaries in the free air computational grids are located a distance of 23 semi-spans from the origin. The sectional pressure distributions computed in the free air and the tunnel environment at compared for selected wing span stations η=0.250, 0.625 and 0.950 in figure 8. In case of the model with a wing span $b = 0.70 * B$, the pressure characteristics in terms of

(a) b = 0.70*B

(b) b = 0.70*B

(c) b = 0.70*B

(d) b = 0.80*B

(e) b = 0.80*B

(f) b = 0.80*B

(g) b = 0.85*B

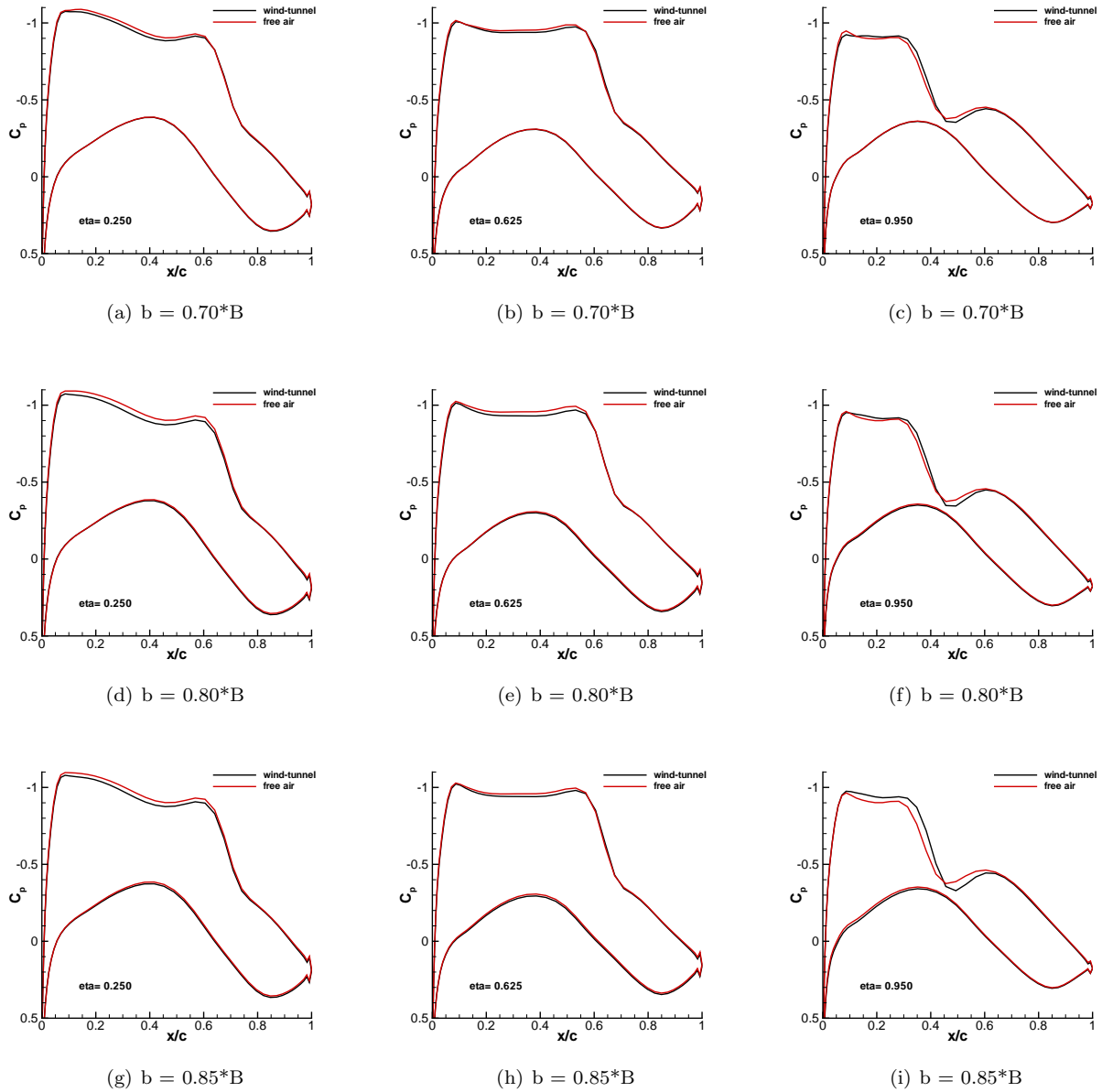(h) b = 0.85*B

(i) b = 0.85*B

Figure 8. Computed effect of wind-tunnel walls on sectional C_p distribution for wing models of various size

leading-edge suction levels and the lower surface pressure distribution compare very well indicating negligible wall-induced incidence angle effects along the span. The shock locations in the free air simulations correspond to the locations in the tunnel solutions. The comparison made for the larger wing model featuring a span of 80% tunnel width shows larger differences in suction plateaus on the inboard wing and small differences start to appear on the pressure side of the outboard wing. In case of the very large wing model having a span

of 85% tunnel width, the side-wall interference effects are evident at wing station η=0.950. An increase in incidence angle is noticed in the leading-edge pressure characteristics in terms of an increase in suction levels. Furthermore, discrepancies are observed for the lower surface pressure distributions which point towards a different location of the stagnation points.

The predicted lift for the models in the tunnel environment is smaller than in the free air simulation which gives the ventilated test section the performance characteristics of an open-jet tunnel. Employing a lift correction based on the C_L/C_D ratio, the predicted drag increment due the tunnel walls at a fixed lift coefficient amounts to 3 and 8 drag counts while traveling from a wing span of 70% tunnel width to a wing span of 80% and 85% tunnel width, respectively.

VI. Conclusions

The development of CFD based interference models for the DNW-HST wind-tunnel is in progress. The ultimate goal is to enable accurate calculations of the transonic flow around test articles in the slotted test section. As a first step, a numerical representation of the wind-tunnel based on multi-block structured grid technology is established which incorporates the slotted test section, the surrounding plenum chamber and part of the diffuser. Exploratory calculations for the empty test section show that measured tunnel calibration data can be reproduced by the CFD simulations. Wind-tunnel wall interference predictions are carried out by calculating the entire wind tunnel flow field including a model of the DLR-F4 wing featuring a wing span of 70%, 80% and 85% of the tunnel width. Comparison of sectional pressure distributions obtained in free air and tunnel simulations for the test article shows consistent wall interference effects with increasing model size. For a constant lift coefficient, the predicted drag increment due the tunnel walls amounts to 3 and 8 drag counts while increasing the model span from 70% tunnel width to 80% and 85% tunnel width, respectively. The present results encourage the inclusion of the model support system in the CFD model in the next development step in order to account for sting interference effects.

References

[1] J.W. Boerstoel, A. Kassies, J.C. Kok and S.P. Spekreijse, "ENFLOW, a full functionality system of CFD codes for industrial Euler/Navier-Stokes flow computations", NLR-TP-96286-L, 1996

[2] S.P. Spekreijse and J.W. Boerstoel, "Multiblock grid generation", NLR-TP-96338-L, 1996

[3] J.C. Kok and S.P. Spekreijse, "Efficient and accurate implementation of the k-ω turbulence model in the NLR multi-block Navier-Stokes system", ECCOMAS 2000, Barcelona, 11-14 September, 2000

[4] F. Wubben, "HST calibration measurements", NLR-TR-94372-L, 1994

[5] S.B. Bernt and H. Sorensen, "Flow properties of slotted walls for transonic test sections", *AGARD-CP-174 Wind-tunnel design and testing techniques*, Paper 17, 1976

[6] J.L. Everhart and P.J. Bobbitt, "Experimental studies of transonic flow field near a longitudinally slotted wind tunnel wall", NASA-TP-3392, 1994